

CMOS Oscillators for Clock Distribution and Injection-Locked Deskew

Masum Hossain and Anthony Chan Carusone, *Senior Member, IEEE*

Abstract—The distribution and alignment of high-frequency clocks across a wide bus of links is a significant challenge in modern computing systems. A low power clock source is demonstrated by incorporating a buffer into a cross-coupled oscillator. Because the load is isolated from the tank, the oscillator can directly drive 50-Ohm impedances or large capacitive loads with no additional buffering. Using this topology, a quadrature VCO (QVCO) is implemented in 0.13 μm digital CMOS. The QVCO oscillates at 20 GHz, consumes 20 mW and provides 12% tuning range. The measured phase noise is -101 dBc/Hz @ 1 MHz frequency offset. A clock alignment technique based upon injection-locked quadrature-LC or ring oscillators is then proposed. Although injection-locked oscillators (ILOs) are known to be capable of deskewing and jitter filtering clocks, a study of both LC and ring ILOs indicates significant variation in their jitter tracking bandwidth when used to provide large phase shifts. By selectively injecting different phases of a quadrature-LC or ring VCO, this problem is obviated resulting in reduced phase noise. The technique is demonstrated using a LC QVCO at 20 GHz while burning only 20 mW of power and providing an 8 dB improvement in phase noise. A ring oscillator deskews a 2 to 7 GHz clock while consuming 14 mW in 90 nm CMOS.

Index Terms—Clock deskew, injection locking, jitter filtering, Q-VCO, ring oscillator.

I. INTRODUCTION

THE energy efficiency of high-speed parallel I/Os is limited by the power consumption of the clocking circuits including clock source, buffers, delay elements and duty cycle correctors. To reduce the power consumption per link, a shared clock source may be used where the phase of the VCO is locked to an external low-jitter [1], [2]. Due to the significant capacitive loading on the clock distribution network, several CML and CMOS inverters are used as buffers [3]. In this work, we propose a VCO with an inherent buffer that re-uses the VCO bias current and provides large driving capacity without additional power consumption. Section II will discuss low power VCO architectures: Colpitts, cross-coupled and proposed VCO. Implementation and experimental results will also be given in this section.

Manuscript received December 01, 2008; revised April 01, 2009. Current version published July 22, 2009. This work was supported by Intel. Fabrication services were provided by Gennum Corporation and Canadian Microelectronic Corporation (CMC).

The authors are with the Department of Electrical and Computer Engineering, University of Toronto, Toronto, Ontario, Canada, M5S 3G4 (e-mail: masum@eecg.utoronto.ca; tcc@eecg.utoronto.ca).

Color versions of one or more of the figures in this paper are available online at <http://ieeexplore.ieee.org>.

Digital Object Identifier 10.1109/JSSC.2009.2022917

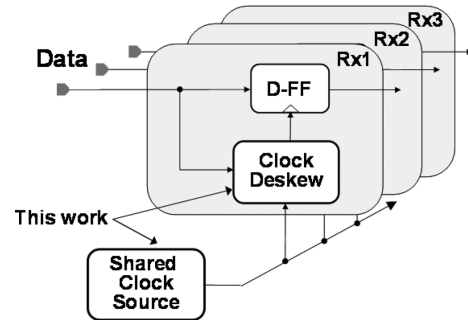


Fig. 1. Shared clocking for high density I/O [1]–[4].

Each link's receiver must compensate for the link's skew with a deskew circuit [4], [5] (Fig. 1). Apart from phase alignment, the deskew block also provides amplification, duty cycle correction and jitter filtering to recover high quality clock. An injection locked oscillator (ILO) is an efficient way of providing all these functionalities; by detuning the oscillator's free-running frequency away from the input frequency, a controlled phase shift is introduced to the clock path [6]. A problem with this approach has been that for large phase shifts considerable variation is observed in the jitter tracking bandwidth and output clock amplitude [7]. In this work, by selectively injecting either one or the other side of a quadrature VCO (QVCO), the required phase adjustment range is cut in half. Section III will provide some theoretical ground work for ILO-based clock deskewing, demonstrating that the variation in jitter tracking bandwidth is fundamental to both LC and ring ILOs. Following that, Section IV will discuss the deskew technique including experimental results for both LC and ring oscillators.

II. LOW POWER VCO ARCHITECTURE

We will first discuss two existing LC VCO topologies: cross-coupled and Colpitts. Finally, the proposed architecture which combines the benefit of both topologies will be discussed.

A. Cross-Coupled Oscillator

A cross-coupled LC VCO topology and its equivalent half circuit is shown in Fig. 2. Here, the ideal gain of -1 is furnished by the cross-coupling to provide a negative resistance of $-g_m$. The tank consists of an inductor L and tunable capacitance C_{var} . The tank loss is mainly dominated by the inductor series resistance R_S which also determines the inductor quality factor $Q_L = \omega L/R_S$. The series resistance R_S can be converted to

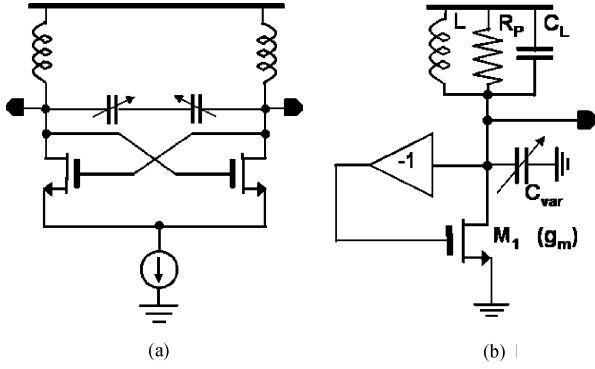


Fig. 2. (a) Conventional cross-coupled LC VCO. (b) Equivalent half circuit.

its parallel equivalent, $R_P = (Q_L^2 + 1)R_S$. To meet the oscillation condition, the negative resistance must compensate the tank loss:

$$g_m \geq \frac{1}{R_P} \approx \frac{Q_L}{\omega_0 L (Q_L^2 + 1)} \quad (1)$$

In the above expression Q_L is the quality factor at the resonance frequency, ω_0 . Assuming this condition is met, the oscillation frequency is determined by the inductance and the capacitance of the tank

$$\omega_0 \approx \frac{1}{\sqrt{LC_{eq}}} = \frac{1}{\sqrt{L(C_{var} + C_L)}}. \quad (2)$$

Here, C_L models any additional capacitance connected to the tank node. The tank amplitude (V_{tank}) is related to the dissipated energy at the tank (E_{tank}) by the energy conservation theorem

$$V_{tank}^2 = \frac{2E_{tank}}{C} = 2E_{tank}\omega_0^2 L. \quad (3)$$

The expression indicates that in the current limited region, for a given energy, tank swing increases with inductance. The design and optimization of cross-coupled oscillators are governed by above (1)–(3). As explained in [8], for a given frequency (i.e., LC_{eq} constant), increasing L/C_{eq} results in higher tank impedance at resonance and as a result oscillation amplitude increases. Thus one can maximize L/C_{eq} ratio to achieve larger tank swing, lower phase noise and lower power consumption [8]. This optimization technique is useful until the oscillator's voltage swing is limited by supply headroom constraints. Beyond that, increasing L/C_{eq} can degrade VCO performance [9]. However, applying this approach to a 20+ GHz VCO design in $0.13 \mu\text{m}$ CMOS results in a very small C_{eq} . Since most of C_{eq} will be consumed by the load capacitance C_L , the varactor must be made small resulting in small tuning range [10]. On the other hand, reducing the L/C_{eq} ratio significantly compromises tank amplitude, phase noise and power consumption. An additional buffer stage is often used to reduce C_L at the cost of additional power consumption.

B. Colpitts VCO

Colpitts VCOs, are widely used in wireless applications due to their robustness to parasitics. Fig. 3 shows the single

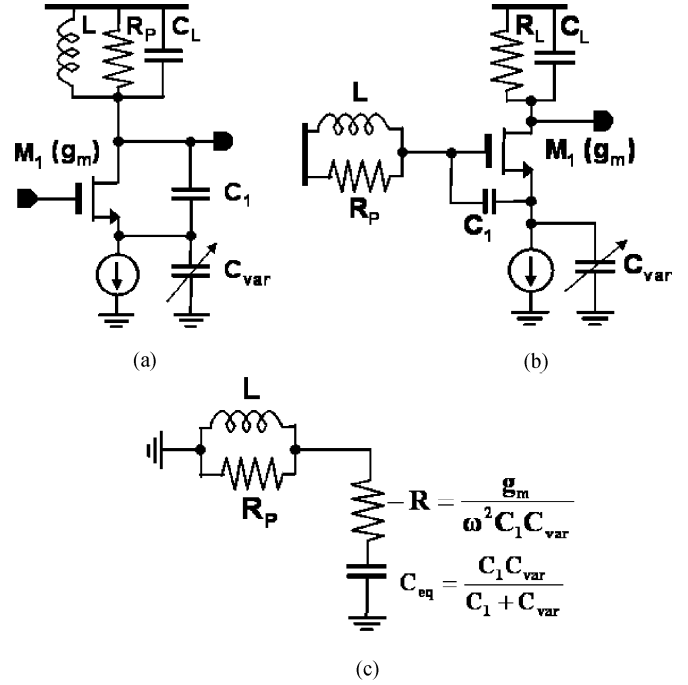


Fig. 3. (a) Conventional Colpitts VCO. (b) Modified Colpitts VCO. (c) Equivalent half circuit.

ended implementation of two variants of the Colpitts VCO: Fig. 3(a) is the well known conventional Colpitts and Fig. 3(b) is a CMOS implementation of the bipolar microwave oscillator discussed in [11]. The implementation in Fig. 3(b) provides inherent buffering [11]: the tank is coupled to the load only through C_{GD} , whereas, in Fig. 3(a) the load capacitance (C_L) is directly across the tank. This is the main advantage of this modified Colpitts VCO. Considering g_m as the small-signal transconductance of M_1 and ignoring the effect of C_{GD} , the input impedance (Z_{in}) looking into the gate of M_1 can be written as

$$Z_{in} = \frac{-g_m}{\omega^2 C_1 C_{var}} + \frac{1}{j\omega} \left(\frac{1}{C_1} + \frac{1}{C_{var}} \right). \quad (4)$$

This leads to the equivalent circuit representation as shown in Fig. 3(c). If R_S models series tank losses, the condition to ensure oscillation of the Colpitts VCO is

$$\frac{g_m}{\omega^2 C_1 C_{var}} \geq R_S. \quad (5)$$

The frequency of oscillation can also be derived from the equivalent circuit shown in Fig. 3(c):

$$\omega_o \approx \frac{1}{\sqrt{LC_{eq}}} = \frac{1}{\sqrt{L \frac{C_1 C_{var}}{C_1 + C_{var}}}}. \quad (6)$$

Note that, unlike the cross-coupled topology, the oscillation frequency is independent of load capacitance (C_L), which signifies the inherent buffering of the modified Colpitts oscillator. The oscillation condition can be written as a function of the equivalent parallel resistive losses R_P

$$g_m \geq \frac{\omega_o^2}{R_P} L (C_1 + C_{var}). \quad (7)$$

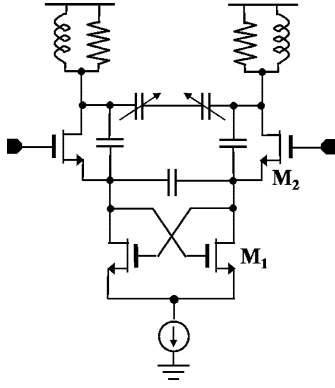


Fig. 4. Colpitts VCO in [12].

Combining (6) and (7), the oscillation condition can be written as

$$g_m \geq \frac{1}{R_P} \frac{(C_1 + C_{var})^2}{C_1 C_{var}}. \quad (8)$$

The factor $(C_1 + C_{var})/(C_1 C_{var})$ can be minimized by choosing $C_1 = C_{var}$, which leads to the minimum required transconductance to ensure oscillation: $g_m = 4/R_P$. Compared to the cross-coupled topology, the Colpitts oscillator requires $4 \times$ additional transconductance which translates into significant additional power consumption. This becomes a concern in wireline applications such high-speed I/Os, where typically the inductor Q is less than 5.

In summary, the Colpitts topology provides good tuning range and output power but consumes a lot of power. On the other hand, cross-coupled VCOs consume less power, but require an additional buffer and are more susceptible to load parasitics [13].

C. Proposed VCO

Cross-coupled and Colpitts VCOs have been previously combined in [12] as shown in Fig. 4. In [12], the bottom cross-coupled pair is used to relax the oscillation condition and improve noise performance. However, note that the tank in this case incorporates the VCO's output node making it impossible for this topology to be used to directly drive large capacitive or small-resistance loads. The circuit behaves basically as a Colpitts oscillator with improved noise performance. In this work the oscillations are sustained mainly by M_1 which is designed to contribute larger negative resistance than M_2 , hence it primarily behaves as a cross-coupled oscillator but the tank buffered from the load by M_2 .

In this work we proposed the topology shown in Fig. 5, which combines the useful properties of both Colpitts and cross-coupled VCO topologies: the inherent buffering of the Colpitts VCO and the low-power oscillation of the cross-coupled VCO. In this architecture, transistor M_2 is introduced in the tank to provide several functionalities: (a) as in the modified Colpitts topology, it decouples the LC tank from the load capacitance; (b) it provides a negative resistance which relaxes the oscillation condition and improves the effective Q of the tank; and (c) unlike the cross-coupled oscillator, the buffer capacitance C_{GS} is in series with C_{var} . For small C_{var} and

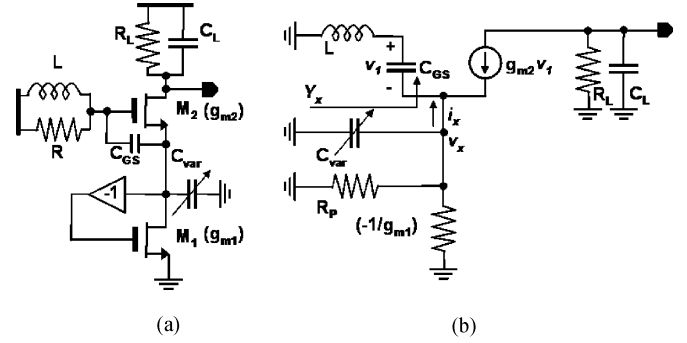


Fig. 5. (a) Proposed VCO. (b) Equivalent half circuit.

C_{eq} , as in the case of 20+ GHz VCOs, this combination can absorb more buffer capacitance and still maintain the required tuning range. Effectively, M_2 serves as a buffer which can directly drive 50-ohm or large capacitive loads. Since it uses the same VCO bias current, there is no additional DC power consumption. Output signal swing is determined by the VCO current and load impedance. $R_L = 50 \Omega$ provides direct output matching at the cost of headroom. If higher output swing is required, high impedance tuned load can be used. To maximize the swing and to avoid additional noise contribution, we do not include a current source in the bottom of the cross-coupled differential pair [8]. This poses no problem if the power supply is well decoupled or regulated.

To identify the effect of M_2 on tank impedance, the equivalent circuit is drawn in Fig. 5(b), from which the following nodal equations may be written:

$$i_x = -v_1(g_{m2} + sC_{GS}) \quad (9a)$$

$$v_x = -v_1(1 + s^2LC_{GS}). \quad (9b)$$

The equivalent admittance looking into the source of M_2 is

$$y_x = \frac{i_x}{v_x} = \frac{g_{m2} + sC_{GS}}{1 + s^2LC_{GS}}. \quad (10)$$

If R_P models total tank losses, the equivalent tank admittance is

$$y_{tank} = y_x + y_{varactor} + y_{loss} \approx \frac{g_{m2} + s(C_{GS} + C_{var} + s^2LC_{GS}C_{var})}{1 + s^2LC_{GS}} + \frac{1}{R_P}. \quad (11)$$

At resonance, the tank admittance must be real. Thus, the oscillation frequency can be found by equating the imaginary part to zero

$$\omega_{osc} = \frac{1}{\sqrt{LC_{eq}}} = \frac{1}{\sqrt{L \frac{C_{GS}C_{var}}{C_{GS} + C_{var}}}}. \quad (12)$$

To sustain oscillation at this frequency, the bottom cross-coupled transistors must provide sufficient negative resistance to overcome the tank losses

$$g_{m1} + \frac{C_{var}}{C_{GS}}g_{m2} \geq \frac{1}{R_P}. \quad (13)$$

This oscillation condition is same as the cross-coupled case with one additional factor: the negative resistance contributed by g_{m2} , which allows additional power savings. Note that there are

two sources of negative resistance here: the bottom cross-coupled pair provide a negative transconductance, $-g_{m1}$ and the top transistors M_2 provide $-(C_{var}/C_{GS})g_{m2}$. As a result this oscillator has two possible modes of operation: (i) as a Colpitts VCO, when the negative resistance provided by M_2 is sufficient to compensate the tank losses, similar to [12]; or (ii) as a cross-coupled VCO, when the negative resistance due to M_1 dominates the oscillation condition. The cross-coupled mode of oscillation requires less power consumption, and hence is the main focus of this work. In this configuration C_{var}/C_{GS} is chosen to provide sufficient tuning range and M_2 is sized such that its gate drain capacitance is small enough to isolate the tank from the output nodes. As a result, the negative resistance of the top transistors is less than 30% of that contributed by the bottom pair.

The effective quality factor (Q_{tank}) for this equivalent tank can be expressed as

$$Q_{tank} \approx \frac{Re\{Z_{tank}\}}{\omega_o L} = \frac{1}{\omega_o L \left(\frac{1}{R_P} - \frac{C_{var}}{C_{GS}} g_{m2} \right)}. \quad (14)$$

It is useful to express this effective tank quality factor in terms of inductor quality factor $Q_L = \omega_o L / R_S$.

$$Q_{tank} \approx \frac{Q_L}{1 - R_P \frac{C_{var}}{C_{GS}} g_{m2}}. \quad (15)$$

Note that, in the absence of transistor M_2 ($g_{m2} = 0$), the tank quality factor is equal to the inductor quality factor. However, in the presence of M_2 , it is possible to improve the tank quality factor well beyond Q_L . For example, consider a 500 pH inductor with a quality factor of 4 used to design a 20 GHz VCO. Choosing $C_{var}/C_{GS} = 0.25$ and $g_{m2} = 10$ mS, we can improve the tank Q beyond 10, which results in a $2.5 \times$ improvement in tank swing. This is particularly useful when designing LC-VCOs in digital CMOS process, where the lossy substrate limits the inductor Q to approximately 4 or 5. For comparison, the proposed tank is simulated with and without g_{m2} as shown in Fig. 6. Note that, the improvement in tank amplitude is a direct effect of the improved quality factor. Using similar approach as described in [14], oscillation amplitude can be derived from Fig. 5(b). In the current limited region, the single ended amplitude of the voltage across the inductor can be written as

$$V_G \approx \frac{2}{\eta\pi} \left(\frac{1}{\frac{1}{R_P} - \frac{\eta}{1-\eta} G_{M2eff}} \right) I_{DC} \quad (16)$$

$$\eta = \frac{C_{var}}{C_{GS} + C_{var}}. \quad (17)$$

Here, G_{M2eff} is the large signal effective transconductance of the transistor M_2 . The voltage across gate and source terminal of M_2 can be written as

$$V_{GS} \approx \frac{2(1-\eta)}{\eta\pi} \left(\frac{1}{\frac{1}{R_P} - \frac{\eta}{1-\eta} G_{M2eff}} \right) I_{DC}. \quad (18)$$

Simulated oscillation amplitude is in good agreement (within 15%) with these two expressions. The simulated phase noise of this 20 GHz VCO at 1 MHz offset was -105 dBc/Hz. The major noise contributors are summarized in Table I. Simulation

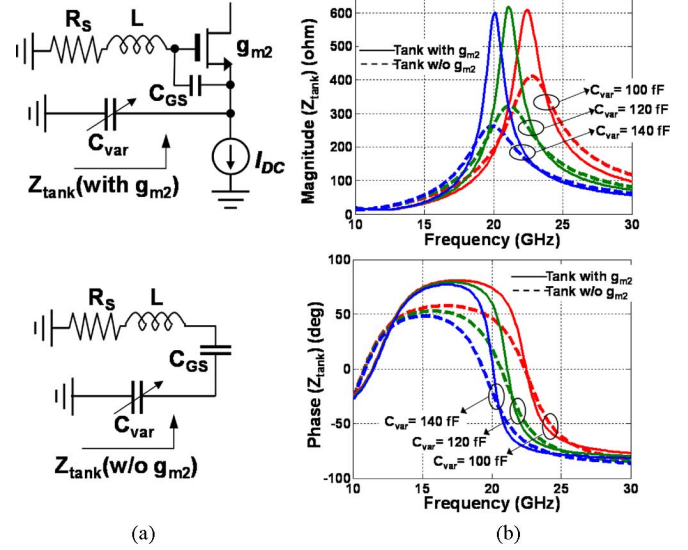


Fig. 6. (a) Simulated tank with and without g_{m2} . (b) Equivalent tank impedance (magnitude and phase) over the tuning range.

TABLE I
PHASE NOISE CONTRIBUTION OF EACH NOISE SOURCE

Noise Source	Contribution
(M_1)	42%
Inductor Loss	28%
(M_2)	20%
Varactor	6%

results also demonstrate that a $\pm 20\%$ variation in C_{var} is sufficient to provide greater than 10% tuning range. To study the effectiveness of M_2 as a buffer, we observed the VCO performance over a large variation of load capacitance from 100 fF to 1 pF. For $M_2 = 16 \mu\text{m}$, the frequency variation is only 50 MHz, the phase noise variation is less than 0.5 dB, and the oscillation amplitude varies less than 3%. However, as we increase the size of M_2 , its effectiveness as a buffer degrades. As shown in Fig. 7, for $M_2 = 30 \mu\text{m}$, a load capacitance variation from 100 fF to 1 pF results in 200 MHz variation in frequency, 1.5 dB variation in phase noise and 7% variation in oscillation amplitude. Variation in the value of R_L from 10 to 70 ohm has even less effect than variations in C_L . Larger values of R_L will result in headroom issues. A comparison of key VCO parameters for all three topologies is summarized in Table II, which supports the qualitative discussion: the proposed VCO essentially combines the benefits of both the cross-coupled and Colpitts topologies.

D. QVCO Implementation

Three existing methods for generating quadrature clock signals are: 1) a VCO followed by C-R, R-C filters, 2) a differential VCO of twice the frequency followed by rising- and falling-edge triggered dividers, and 3) a Q-VCO formed by coupling two differential VCOs. The first technique results in significant additional power consumption in the buffers driving the passive filter. The second technique requires the design of a 40 GHz VCO and dividers in $0.13 \mu\text{m}$ digital CMOS which would be difficult and power consuming. Thus

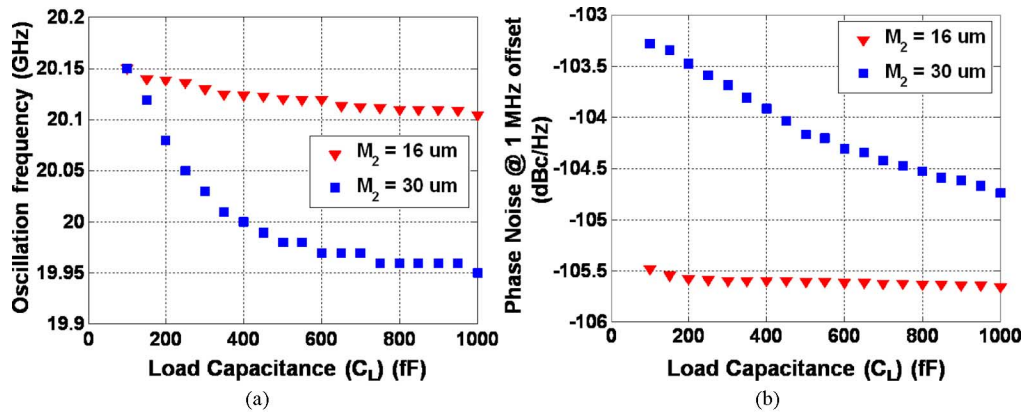


Fig. 7. Effect of load capacitance variation on (a) oscillation frequency and (b) phase noise.

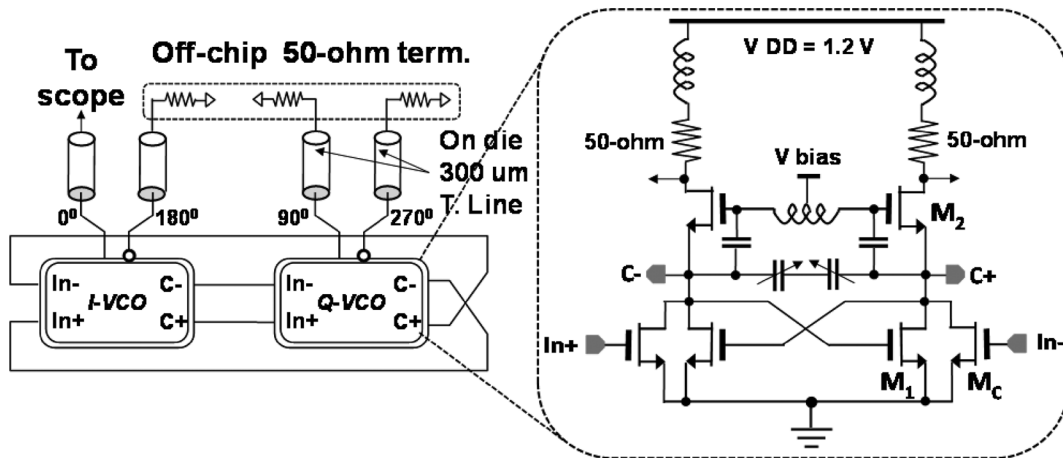


Fig. 8. Implementation of QVCO architecture, test set up and detail schematic of QVCO.

TABLE II
VCO TOPOLOGY SUMMARY

	Frequency of Oscillation	Minimum Required g_m	Tank Quality Factor
Cross-Coupled	$f_{osc} = (2\pi\sqrt{L(C_{var} + C_L)})^{-1}$	$\geq \frac{1}{R_P}$	$Q_{tank} \approx Q_L$
Colpitts	$f_{osc} = (2\pi\sqrt{L\frac{C_1 C_{var}}{C_1 + C_{var}}})^{-1}$	$\geq \frac{4}{R_P}$	$Q_{tank} \approx Q_L$
Proposed VCO	$f_{osc} = (2\pi\sqrt{L\frac{C_{GS} C_{var}}{C_{GS} + C_{var}}})^{-1}$	$\geq (\frac{1}{R_P} - \frac{C_{var}}{C_{GS}} g_{m2})$	$Q_{tank} \approx \frac{Q_L}{1 - R_P \frac{C_{var}}{C_{GS}} g_{m2}}$

for quadrature signal generation at 20 GHz, we focus on the third approach: a Q-VCO. A quadrature version of the proposed VCO is implemented by coupling two differential VCOs operating at the same frequency. In-phase coupling, with a coupling factor greater than 0.25, ensures quadrature phase generation. Coupling was provided using additional devices M_C (Fig. 8). Quadrature (4-phase) VCOs in general have several disadvantages compared to their differential (2-phase) counterparts: a) due to the additional DC power consumption in the coupling devices, the power consumption of a quadrature VCO is usually more than twice the power consumption of a differential VCO at the same frequency; b) in the quadrature implementation, both tanks operate slightly off resonance due to mismatch which results in higher phase noise and reduced tank impedance compared to a differential implementation.

This QVCO is implemented in $0.13 \mu\text{m}$ digital CMOS, typical for high speed I/Os (Fig. 9). There were five metal layers available with the top layer being less than $1 \mu\text{m}$ thick. Poly,

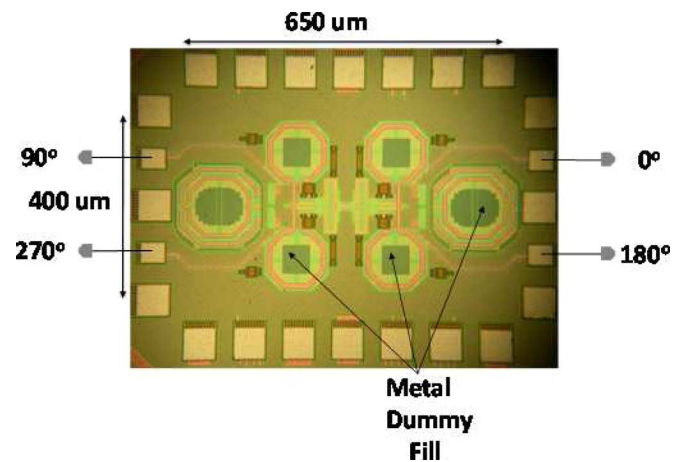


Fig. 9. Die photo of the implemented Q-VCO in $0.13 \mu\text{m}$ CMOS.

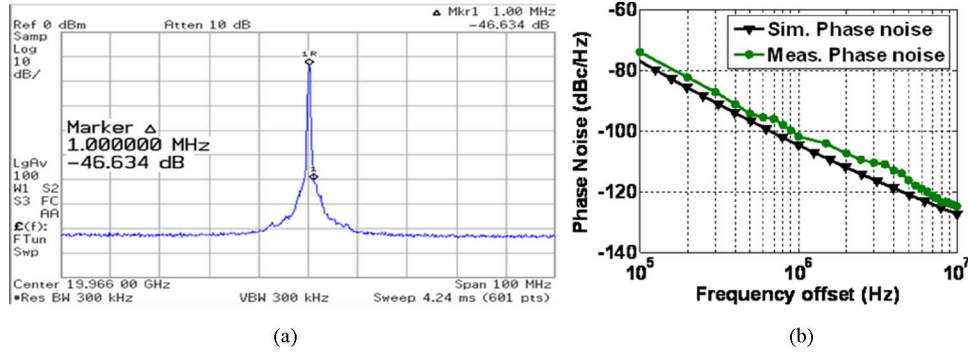


Fig. 10. (a) Measured spectrum at 20 GHz. (b) Simulated and measured phase noise of the Q-VCO at 20 GHz.

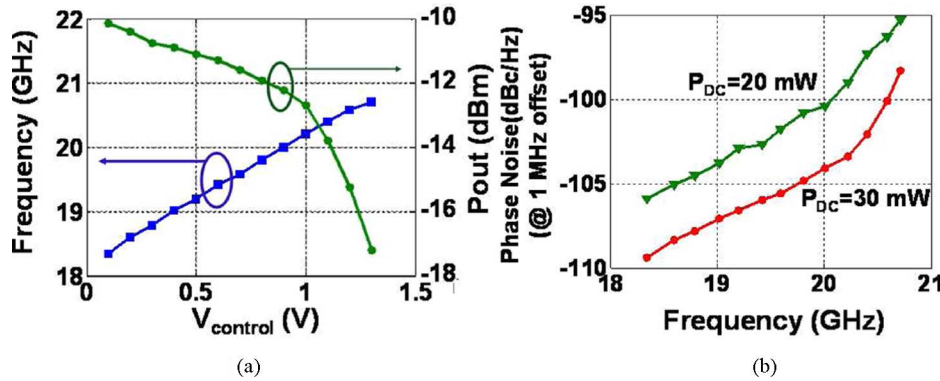


Fig. 11. Summary of VCO performance. (a) Measured tuning range output power and (b) phase noise of the Q-VCO at different frequencies.

metal 1 and metal 2 is used as metal fill under the inductor and all metal layers (1–4) except metal 5 are used inside the inductor loop to meet the metal density. Both the single turn inductor used in the tank and the inductor in the load is built with the top Metal layer, metal 5. For a 500 pF inductor, a Q of 4 was achieved which translates to an R_P of 267 Ω . C_{GS} and C_{var} were chosen to be 360 fF and 140 fF respectively, which provide an equivalent capacitance of 100 fF. The minimum transconductance required to meet the oscillation condition was found to be 5 mS. With some safety margin, a transconductance of 10 mS was chosen with each transistor ($W_1 = 16 \mu\text{m}$) consuming 3 mA of current. Each coupling device M_C ($W_C = 5 \mu\text{m}$) consumes another 1 mA of current. Taking advantage of the transistor M_2 , no additional buffer is used and the VCO directly drives on-chip 50-ohm termination in parallel with 50-ohm off-chip termination. A 300- μm length of transmission line connects the VCO outputs to probe pads. The complete Q-VCO consumes 16 mA of current from a 1.2 V supply and it can provide a clock swing of 200 mV peak-to-peak per side across 25 ohm effective loads. For comparison, we designed both Colpitts and cross-coupled VCO with the same inductor and equivalent tank capacitances. The Colpitts VCO consumed four times additional power resulting in a total power consumption of 100 mW. On the other hand, the cross-coupled VCO consumed the same power as the proposed one. However, to provide the same swing at the load, an additional CML buffer was required, consuming an additional 16 mA of current and thus raising the total power consumption to 50 mW. Furthermore, the cross-coupled VCO had a lower tuning range because the

buffer's input capacitance is in parallel to the tuning capacitor and thus dominates the tank capacitance [10].

E. Measured Results

Measured results of the QVCO are summarized in Figs. 10 and 11. The VCO can be tuned from 18.3 GHz to 20.75 GHz providing 12% tuning range. Including the on-die transmission line and pad, the total output load capacitance is estimated at 220 fF. The per-side output power measured in a 50-ohm environment varied from -11.5 dBm to -17.5 dBm over the tuning range. The reduced output power at higher frequency is due to reduced load impedance and reduced tank impedance. This also significantly increases phase noise. A captured spectrum, the measured and simulated phase noise at 20 GHz is shown in Fig. 10. The phase noise over the tuning range is also shown in Fig. 10. For comparison, key performance metrics for different VCO topologies are summarized in Table III. According to the ITRS 2003[15], the figure-of-merit for VCOs is

$$\text{FoM} = 10 \log_{10} \left(\left(\frac{f_{\text{osc}}}{\Delta f} \right)^2 \frac{1}{L(\Delta f) P_{\text{diss}} (\text{mW})} \right). \quad (19)$$

Our earlier conclusion regarding Colpitts and cross-coupled VCOs are in good agreement with the measured results from [13]: cross-coupled VCOs can achieve a significant advantage over Colpitts VCOs for low-power applications. However, this advantage is significantly compromised when the buffer is included in the performance metric. In addition, as pointed out

TABLE III
COMPARISON OF STATE-OF-ART CMOS VCOS

	[10]	[13]	[13]	[16]	[17]	This Work
	JSSC'07	CSICS'06	CSICS'06	JSSC'04	VLSI'05	
Technology	0.13-um CMOS	90-um CMOS	90-um CMOS	0.13-um CMOS	90-um SOI	0.13-um CMOS
Frequency	26GHz	10GHz	10GHz	10GHz	40GHz	20GHz
Topology	G_m Tuned	Colpitts	Cross- Coupled	Cross- Coupled	Cross- Coupled	Proposed VCO
Diff./Quadrature	Diff.	Diff.	Diff.	Quad.	Quad.	Quad.
Tuning Range	23.6%	12.2%	15.8%	15%	12.5%	12%
Inductor Q/ Transformer Q	18	10	10	—	18	5
Phase Noise (dBc/Hz@1MHz)	-92.6	-117.5	-109.2	-95	-87 @ 3MHz	-101
VCO Power	43.6mW	36mW	7.5mW	14.4mW	—	—
VCO+ Buffer	50mW	—	17.5mW	—	81mW	20mW
FOM (VCO) (dB)	163.9	181.9	180.4	163.4	—	—
FOM (VCO+ Buffer)	163.3	—	176.5	—	150.4	174.01

in the previous section, there is significant performance degradation in cross-coupled QVCOs compared to their differential counterparts [16], [17]. Although the inductor Q in this VCO is much lower compared to the other VCOs listed in the table, this VCO topology still has a FoM better than other QVCOs in CMOS. The differential 10 GHz Colpitts VCO designed in [13] consumes more power than the 20 GHz QVCO designed in this work, which demonstrates the low power advantage of the proposed topology. The current consumption of the QVCO is set by the gate voltage of transistor M_2 . Keeping the same supply voltage of 1.2 V, power consumption can be increased from 20 mW to 30 mW which results in 5 dB reduction in phase noise (Fig. 11).

III. DESKEW WITH INJECTION LOCKING

Historically, injection locking has been used for low power frequency division [18]. More recently, ILOs are also used as a jitter filter on high-frequency clocks [19] and as a clock deskew element [6], [7]. Compared to traditional voltage-control delay elements, ILO-based deskew provides several advantages: (a) due to its high sensitivity, ILOs can operate with very small input amplitude – thus the reference clock can be distributed with low power; (b) since an ILO behaves as a first order PLL, it rejects high frequency jitter and is less susceptible to power supply noise; (c) the clock can be deskewed by detuning the free running frequency of the ILO. To cover an entire clock period, the required deskew range should be at least $\pm 180^\circ$. Assuming that phase-inversion of a differential ILO may be trivially accommodated, a deskew range of $\pm 90^\circ$ is required.

Present ILO-based deskew techniques have several disadvantages. For small injected signals, the deskew range is less than $\pm 90^\circ$ [7]. With large injection strength, it is possible to extend the deskew range but this requires a wide tuning range in the ILO. Furthermore, providing skews near 90° results in considerable variation in the jitter tracking bandwidth and output clock

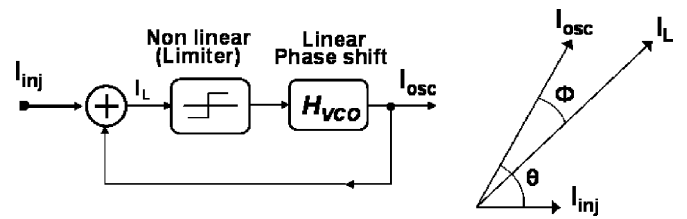


Fig. 12. ILO model and corresponding vector diagram.

amplitude [7]. Previous theoretical studies on ILOs have focused on their lock range and the behavior of an ILO outside its lock range for both small injection [20] and large injection [21]. In this work we are specifically interested in the phase noise (and jitter) of the deskewed clock. We seek a general treatment applicable to both LC and ring VCOs.

With that motivation, we adopt the ILO model shown in Fig. 12 for any injection method and oscillator topology [18], [21]. Here, H_{VCO} is the VCO's small-signal open loop frequency response and will depend on the VCO topology. In the case of an LC oscillator, H_{VCO} is a tuned response, whereas, in case of a ring oscillator, H_{VCO} is a low pass response. Nonlinearities associated with the VCOs are taken into account by the nonlinear block. The phasor diagram in Fig. 12 is taken with respect to the injected frequency, ω_{inj} . The oscillator has a free running frequency of ω_0 . Under injection within the oscillator's lock range, the oscillator output frequency drifts from ω_0 and, in steady-state, settles to ω_{inj} . Let its instantaneous oscillation frequency be ω and $\Delta\omega$ is the inherent frequency difference, $\Delta\omega = \omega_0 - \omega_{inj}$. Thus, the oscillator output phasor $I_{osc} = |I_{osc}|e^{j\theta}$ rotates with an instantaneous angular frequency $\omega - \omega_{inj}$. The phasor I_L is the vector summation of I_{inj} and I_{osc} : $I_L = I_{osc} + I_{inj} = |I_L|e^{j(\theta-\Phi)}$. Here, Φ is the phase shift introduced by the H_{VCO} to satisfy the oscillation condition, $\Phi = \angle H_{VCO}(j\omega)$. It was shown in [21] that

$$\tan \Phi = \frac{K \sin \theta}{1 + K \cos \theta} \quad (20)$$

where $K = |I_{inj}|/|I_{osc}|$ is the injection strength. We define

$$A \equiv \frac{\tan \Phi}{\omega_o - \omega}. \quad (21)$$

By noting $\omega - \omega_{inj} = d\theta/dt$ and substituting $\Delta\omega = \omega_o - \omega_{inj}$, this may be rearranged

$$\tan \Phi = -A \left(\frac{d\theta}{dt} - \Delta\omega \right) \quad (22)$$

Equating $\tan \Phi$ from (20) and (22),

$$\frac{d\theta}{dt} = -\frac{1}{A} \frac{K \sin \theta}{(1 + K \cos \theta)} + \Delta\omega. \quad (23)$$

This is the same locking equation used in [20] and [21], but generalized so that all oscillator-topology dependence is captured by A . For the parallel RLC resonant tank [20], [21],

$$A = \frac{2Q}{\omega_o} \quad (24)$$

where Q is the quality factor of the tank circuit. For an LC resonant tank with resistive losses in series with the inductor, the appropriate value of A is [22]

$$A = \frac{Q}{\omega_o} \left(1 - \frac{1}{Q^2} \right)^{1.5} \left(\frac{\omega + \omega_o}{\omega_o^2} \right) \omega. \quad (25)$$

A simpler definition of A may be obtained by taking a first-order expansion of $\tan \Phi$ around $\omega = \omega_o$ in (18). Since ω_o is the oscillator's free-running frequency, $\tan \Phi = 0$ at $\omega = \omega_o$. Hence,

$$A \cong -\left. \frac{d \tan \Phi}{d\omega} \right|_{\omega=\omega_o}. \quad (26)$$

The accuracy of this approximation diminishes as $\Delta\omega$ increases. For a ring oscillator, this approximation is used in the Appendix to show that

$$A \cong \frac{n}{2\omega_o} \sin \left(\frac{2\pi}{n} \right) \quad (27)$$

where n is the number of stages in the ring. With these expressions for A , we can use (23) as a general locking equation which is VCO topology-independent.

A. Clock Deskew

Within the lock range, the steady state output frequency will always track the injected frequency, $\omega = \omega_{inj}$, and the phase difference between the injected and ILO output becomes constant, $d\theta/dt = 0$. Making these substitutions into (23),

$$\Delta\omega = \frac{1}{A} \left(\frac{K \sin \theta_{ss}}{1 + K \cos \theta_{ss}} \right) \quad (28)$$

where θ_{ss} is the steady state phase shift between the injected and output clocks. The maximum value of $\Delta\omega$ is obtained when $\cos \theta_{ss} = -K$. Thus, we define lock range as

$$\omega_{LOCK} = \frac{1}{A} \frac{K}{\sqrt{1 - K^2}}. \quad (29)$$

Within lock range ($\Delta\omega < \omega_{LOCK}$) (28) is valid for any value of K and $\Delta\omega$. For small injection strength i.e., $K \cos \theta_{ss} \ll 1$ the above relation can be simplified as [20]

$$\theta_{ss} \approx \sin^{-1} \left(\frac{A}{K} \Delta\omega \right). \quad (30)$$

As (30) suggests, for small frequency offsets the phase shift is approximately linear with respect to $\Delta\omega$. This property is particularly useful for ILO-based clock deskewing. Experimental and simulated deskew curves using the differential VCO topology discussed in the previous section are shown in Fig. 13. For experimental study we AC coupled an external 19 GHz clock to I-VCO only. Deskew curve was generated by detuning I-VCO only. According to (30), the deskew angle θ_{ss} decreases with increasing injection strength K . Note that the validity of (30) is limited to small injection strength (K) only. For larger injection strength we can consider (29) where we see that the lock range increases with injection strength. In particular, larger injection strength increases the usable linear portion of the deskew curve, θ_{ss} vs. $\Delta\omega$. Finally, note that (30) predicts a maximum achievable deskew of $\pm 90^\circ$; however, under very strong injection the approximations in (30) break down and slightly larger deskew angles are, in fact, achievable but accompanied by nonlinearity in the deskew curve and, as we shall see, variations in the jitter tracking bandwidth and oscillation amplitude.

B. Phase Noise Filtering

The transient phase response of the ILO can be obtained by integrating (23) with respect to time resulting in a first-order response [20], [21]

$$\theta(t) = \theta_0 e^{-\omega_P t}. \quad (31)$$

In (31), θ_0 is the phase difference at time $t = 0$ between the free running VCO output and the injected clock. Generalizing the result in [18] to cover different oscillator topologies, ω_P can be estimated as

$$\omega_P = \sqrt{\frac{K^2}{A^2} - \Delta\omega^2}. \quad (32)$$

For weak injection, $K \ll 1$, this simplifies to the same result as in [20], [21], $\omega_P = K/A$. Thus, ILOs are functionally equivalent to a first order PLL [18] where input phase noise is low pass filtered

$$JTF_{INPUT} = \frac{1}{1 + \frac{j\omega_{jitter}}{\omega_P}} \quad (33)$$

and VCO phase noise is high pass filtered

$$JTF_{VCO} = \frac{\frac{j\omega_{jitter}}{\omega_P}}{1 + \frac{j\omega_{jitter}}{\omega_P}}. \quad (34)$$

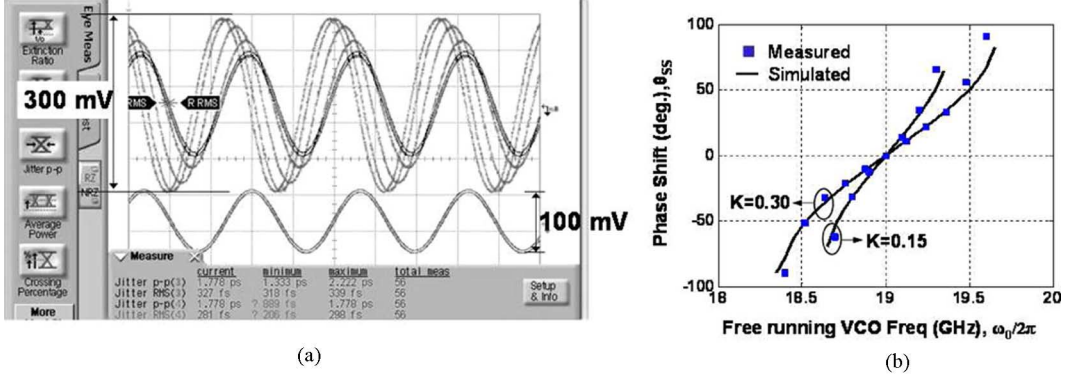


Fig. 13. (a) Captured deskewed clock at different skew setting. (b) Skew curve as a function of free running VCO frequency ($\omega_{inj} = 2\pi \times 19$ GHz).

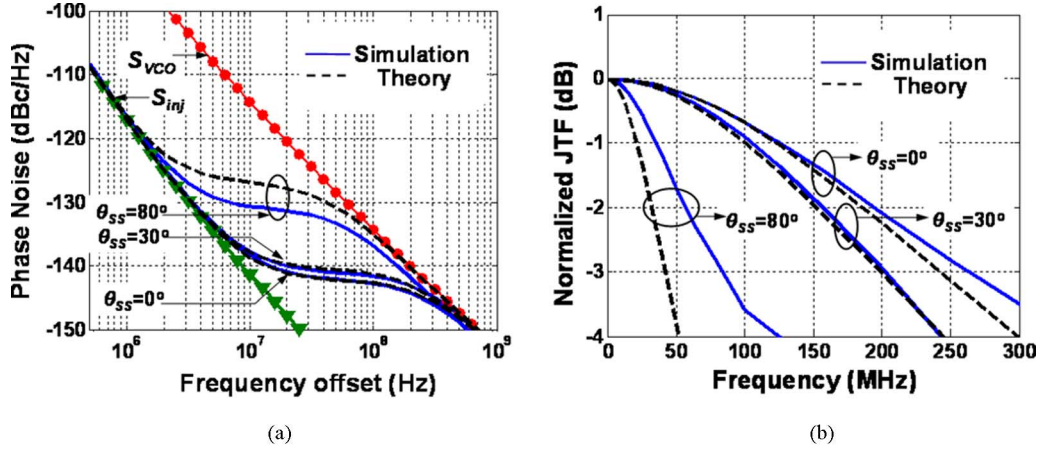


Fig. 14. (a) Simulated and predicted phase noise of the LC VCO at different deskew settings at $\omega_{inj} = 2\pi \times 19$ GHz. (b) Simulated and predicted jitter transfer characteristics at different skew settings $\omega_{inj} = 2\pi \times 19$ GHz. For both simulations $Q = 6$ and $K = 0.15$.

Here ω_{jitter} is the jitter frequency. If S_{inj} is the phase noise of the injected signal and S_{VCO} is the VCO phase noise, then the phase noise of the deskewed clock is

$$S_{out} = |JTF_{input}|^2 S_{inj} + |JTF_{VCO}|^2 S_{VCO}. \quad (35)$$

Using the jitter transfer functions in (33) and (34),

$$\begin{aligned} S_{out}(\omega_{jitter}) &= \frac{\omega_P^2 S_{inj} + \omega_{jitter}^2 S_{VCO}}{\omega_P^2 + \omega_{jitter}^2} \\ &= \frac{\left(\frac{K^2}{A^2} - (\Delta\omega)^2\right) S_{inj} + \omega_{jitter}^2 S_{VCO}}{\frac{K^2}{A^2} - (\Delta\omega)^2 + \omega_{jitter}^2}. \end{aligned} \quad (36)$$

It is also desirable to express the phase noise of the deskewed clock as a function of deskew angle θ_{ss} . This can be done using the relationship between frequency offset and deskew angle:

$$S_{out}(\omega_{jitter}) = \frac{\left(\frac{K}{A}\right)^2 \cos^2 \theta_{ss} S_{inj} + \omega_{jitter}^2 S_{VCO}}{\left(\frac{K}{A}\right)^2 \cos^2 \theta_{ss} + \omega_{jitter}^2}. \quad (37)$$

This phase noise expression for the deskewed clock provides several insights: (a) the jitter tracking bandwidth of the ILO depends upon the frequency offset between the injected and

free running VCO frequency, $\Delta\omega$, and hence upon the deskew angle, θ_{ss} ; (b) Close to the lock range ($\Delta\omega \approx K/A$), $S_{OUT} \approx S_{VCO}$, so no phase noise filtering will be observed. Taking a different approach, the same conclusion was obtained in [23]. In terms of the phase shift, θ_{ss} , effective phase noise filtering is achieved for small deskew angles, but for large deskew angles (e.g., $\theta_{ss} = \pm 90^\circ$) no phase noise filtering is achievable (i.e., $S_{OUT} \approx S_{VCO}$).

The LC VCO discussed in Section II is simulated as an ILO by injecting a relatively low-jitter clock into the tank through a capacitive coupling. The injected clock frequency was 19 GHz and the free-running VCO frequency was detuned away from 19 GHz to obtain phase shifts. The predicted phase noise of the deskewed clock along with the simulated one is shown in Fig. 14(a). For this study a low noise clock is generated and injected to the differential VCO. Normalized jitter transfer functions are shown for different deskew angles in Fig. 14(b). Jitter Tracking Bandwidth (JTB) of the ILO as a function of the frequency offset and injection strength is shown in Fig. 15. The theoretical predictions are based upon a parallel RLC-tank model using the expression for A in (21) with $Q = 6$. For small phase shifts, the theory and simulation results are in good agreement. Increasing discrepancies are observed at larger phase shifts because of the simplified parallel RLC-tank model. Regardless, at $\theta_{ss} = \pm 90^\circ$ very little jitter filtering is observed. This was also

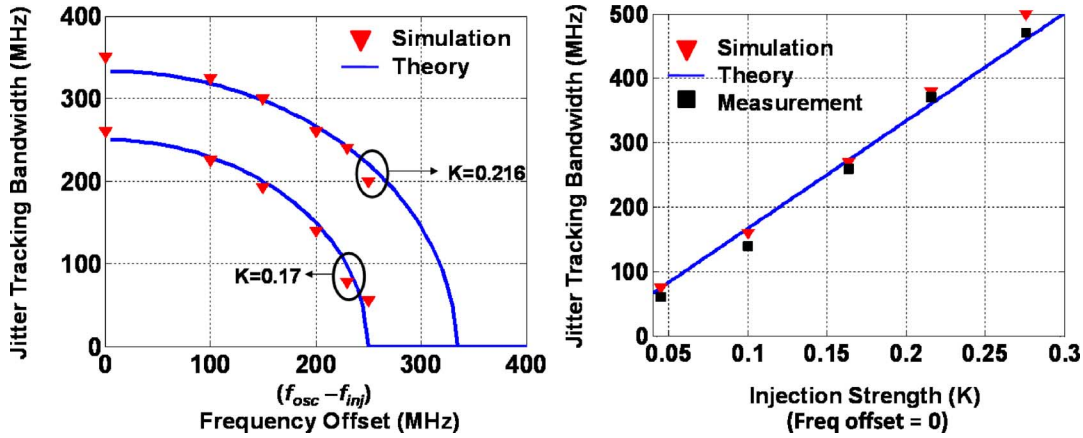


Fig. 15. Variation of jitter tracking bandwidth (JTB) as a function of frequency offset and injection strength, $\omega_{inj} = 2\pi \times 19$ GHz and $Q = 6$.

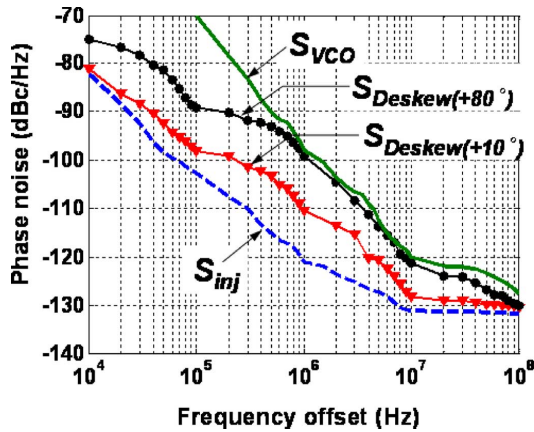


Fig. 16. Measured phase noise plot of the VCO, injected signal and deskewed clock at $\omega_{inj} = 2\pi \times 19$ GHz.

experimentally verified by capturing phase noise plots of the injected signal, free-running VCO, and the deskewed clock under injection locking in Fig. 16.

C. Deskew With Harmonic Injection

Phase deskew can also be achieved when the VCO is injected with a super- or sub-harmonic clock such that $f_{osc} = m f_{inj}$. The phase noise expression in (33) becomes,

$$S_{out}(\omega_{jitter}) = \frac{m^2 \left(\frac{K}{A}\right)^2 \cos^2 m\theta_{ss} S_{inj} + \omega_{jitter}^2 S_{VCO}}{\left(\frac{K}{A}\right)^2 \cos^2 m\theta_{ss} + \omega_{jitter}^2} \quad (38)$$

If the oscillator is injected with m th order sub-harmonic, then the output phase noise will degrade by a factor m^2 within the jitter tracking bandwidth [24]. On the other hand, super-harmonic injection improves the phase noise of the injected signal by m^2 . For example, second harmonic of the oscillation frequency is injected in the tail of the four stage ring oscillator in Fig. 17(a). The phase noise of the deskewed clock and the corresponding jitter tracking bandwidth at different deskew angles is shown in Fig. 17(b)-(c) and compared with theoretical predictions based upon (38), the expression for A derived in the

Appendix. Again theoretical predictions are in good agreement with the simulation results for small deskew phase angles. For large phase shifts, inaccuracies arise due to first-order approximation for A applied in (23).

In summary, the theory, simulation and experimental study of the ILO-based deskew techniques have identified several limitations of existing techniques for large phase deskew angles: (i) the phase steps are non-linear; (ii) the output clock amplitude varies significantly and (iii) there is little or no jitter filtering. However, if we restrict the frequency offset within $|\Delta\omega| < 0.5\omega_{LOCK}$, above-mentioned limitations are not very significant. The derived phase noise expressions are applicable for any ILO topology with appropriate choice of A . The theoretical results are summarized for both ring and LC oscillators in Table IV.

IV. PROPOSED DESKEW TECHNIQUE

In the proposed architecture, a QVCO is used, where we can selectively inject either the in-phase or the quadrature portion of the VCO. This allows us to achieve $\pm 180^\circ$ using only half of the lock range. As a result, both jitter tracking bandwidth and clock amplitude suffers much less variation. This proposed technique can be implemented either with an LC QVCO or using a ring oscillator.

A. Deskew With LC QVCO

The analysis of a differential ILO can be extended for a quadrature ILO as shown in Fig. 18. First we will study the case without injection and then, the effect of injection will be discussed. Due to mutual coupling between the two VCOs, each of them oscillates at a frequency slightly offset from resonance. As a result, in a free running QVCO the tank introduces a phase shift δ_1 between the output voltage V_{Iosc} and current I_{Iosc} . Thus the mutual coupling between these two VCOs can be viewed as injection locking [25] and the general locking (23) can be applied to both the I-VCO and Q-VCO:

$$\frac{d(\theta_I - \theta_Q - \delta_1)}{dt} = -\frac{1}{A} \frac{K_c \sin(\theta_I - \theta_Q - \delta_1)}{1 + K_c \cos(\theta_I - \theta_Q - \delta_1)} \quad (39)$$

$$\frac{d(\theta_Q - \theta_I - \delta_2)}{dt} = -\frac{1}{A} \frac{K_c \sin(\theta_Q - \theta_I - \delta_2)}{1 + K_c \cos(\theta_Q - \theta_I - \delta_2)} \quad (40)$$

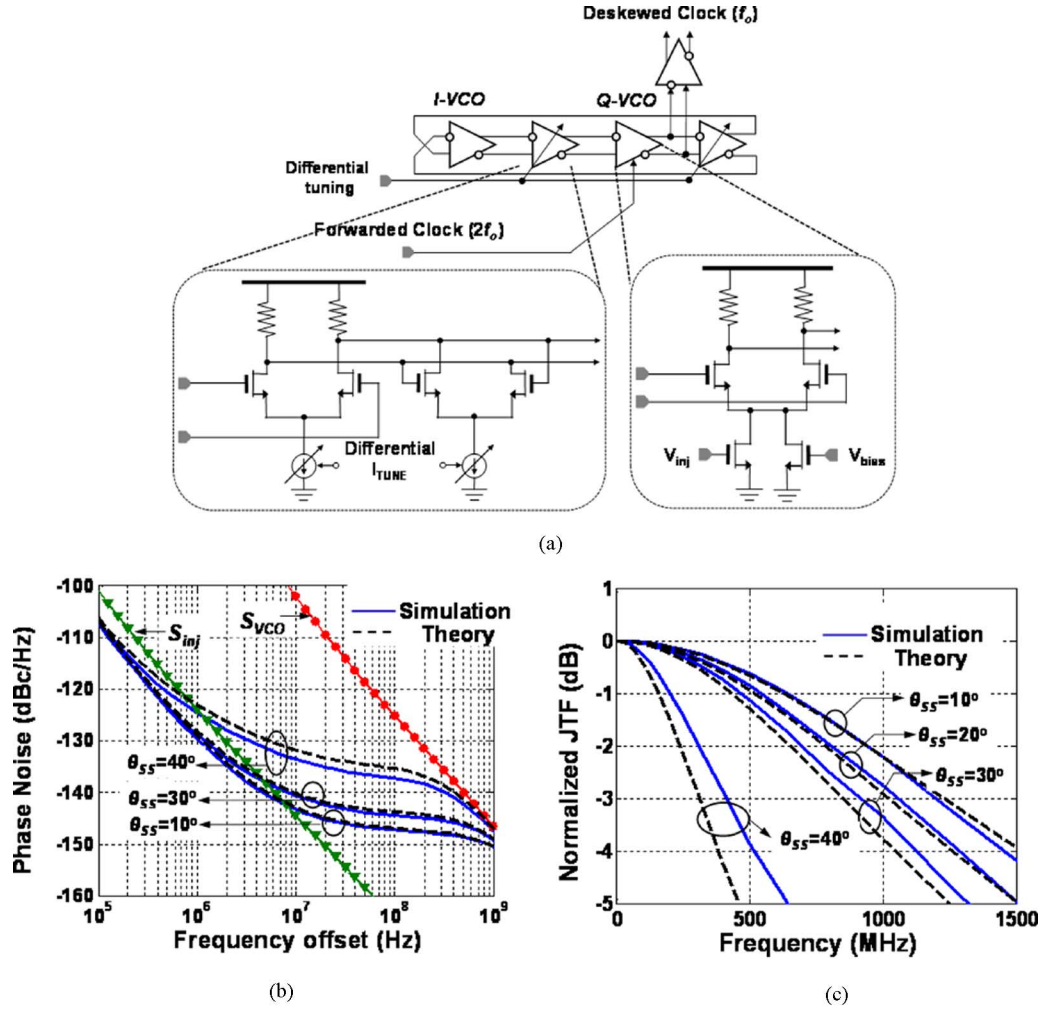


Fig. 17. Deskew with harmonic injection locking. (a) Implemented ring oscillator for deskew. (b) Phase noise at different skew settings at $\omega_{inj} = 2\pi \times 14$ GHz. (c) Jitter transfer characteristics at different skew setting $\omega_{inj} = 2\pi \times 14$ GHz. For both simulations $K = 0.35$, $n = 4$, $\omega_0 = 2\pi \times 7$ GHz and $m = 0.5$.

TABLE IV
SUMMARY OF ILO BASED DESKEW PARAMETERS

	Phase Shift Q_{ss}	Lock Range ω_{LOCK}	Jitter Tracking BW ω_P
Ring Oscillator [n=No. of Stages]	$\sin^{-1}\left[\frac{n(\omega_{inj}-\omega_0)}{2K\omega_0}\sin\left(\frac{2\pi}{n}\right)\right]$	$\frac{2\omega_0}{n}\frac{K}{\sin\frac{2\pi}{n}}\frac{1}{\sqrt{1-K^2}}$	$\sqrt{\left[\frac{2\omega_0 K}{n\sin\frac{2\pi}{n}}\right]^2 - [\omega_{inj} - \omega_0]^2}$
LC Oscillator [Q=Tank Quality Factor]	$\sin^{-1}\left[\frac{2Q[\omega_{inj}-\omega_0]}{K\omega_0}\right]$	$\frac{\omega_0}{2Q}\frac{K}{\sqrt{1-K^2}}$	$\sqrt{\left[\frac{\omega_0 K}{2Q}\right]^2 - [\omega_{inj} - \omega_0]^2}$

Here, we assume that both VCOs are identical (i.e., $\Delta\omega = 0$) and the phase difference between them is $\Delta\theta$ ($\theta_Q - \theta_I = \Delta\theta$). To find the final phase relationship between these two VCOs, we find the steady-state solution of the above equations:

$$\frac{K_c \sin(\Delta\theta - \delta_1)}{1 + K_c \cos(\Delta\theta - \delta_1)} = -\frac{K_c \sin(\Delta\theta + \delta_2)}{1 + K_c \cos(\Delta\theta - \delta_2)}. \quad (41)$$

To further simplify the above equations, we consider two cases:

1) Case : I: , when two loops are strongly coupled, $K_c \approx 1$:

$$\frac{\sin(\Delta\theta - \delta_1)}{1 + \cos(\Delta\theta - \delta_1)} = -\frac{\sin(\Delta\theta + \delta_2)}{1 + \cos(\Delta\theta - \delta_2)}. \quad (42)$$

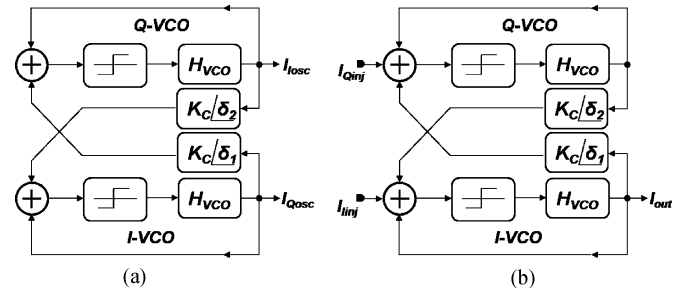


Fig. 18. Proposed phase deskew technique. (a) Q VCO model without injection. (b) QVCO with injection for proposed deskew scheme.

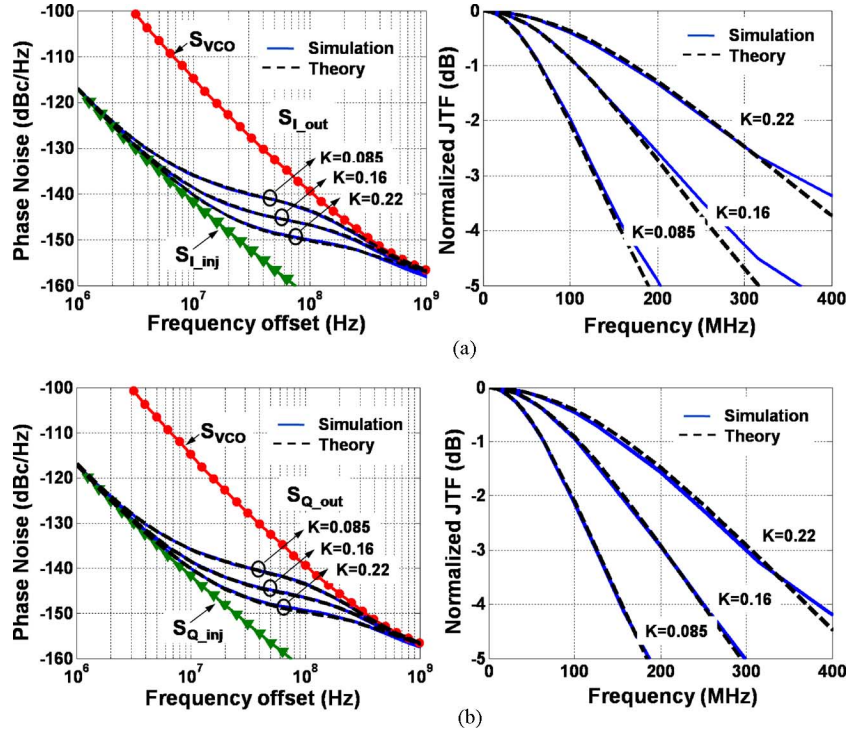


Fig. 19. Theory verification with (a) I-VCO injection, and (b) Q-VCO with injection for $\omega_{inj} = 2\pi \times 20$ GHz. For both simulations $Q = 6$ and mutual injection strength is $K_c = 0.5$.

Substituting $\sin \alpha = 2 \sin(\alpha/2) \cos(\alpha/2)$ and $1 + \cos \alpha = 2 \cos^2(\alpha/2)$:

$$\tan \frac{\Delta\theta - \delta_1}{2} = -\tan \frac{\Delta\theta + \delta_2}{2} \quad (43)$$

$$\delta_1 - \delta_2 = 2\Delta\theta \quad (44)$$

2) Case II: , when two loops are weakly coupled, $K_c \ll 1$:

$$K_c \sin(\Delta\theta - \delta_1) = -K_c \sin(\Delta\theta + \delta_2). \quad (45)$$

This gives us the same relationship as before:

$$\delta_1 - \delta_2 = 2\Delta\theta. \quad (46)$$

For quadrature output such as $\Delta\theta = \pi/2$, $\delta_1 = \delta_2 + \pi$ which leads to well known antiphase coupling. On the other hand in-phase coupling leads to $\Delta\theta = 0$. Traditionally, the antiphase coupling is implemented by simply crossing over the available differential outputs. Thus, δ_1 and δ_2 maintains static phase relationship which allow us to further simplify the differential equation:

$$\frac{d(\Delta\theta)}{dt} = \frac{-1}{A} \frac{K_c \sin(\Delta\theta)}{1 + K_c \cos(\Delta\theta)}. \quad (47)$$

The time domain phase variation between I-VCO and Q-VCO can be obtained by integrating with respect to time:

$$\tan \left(\frac{\Delta\theta}{2} \right) \sin^{K_c}(\Delta\theta) = e^{-K_c t/A} + \psi. \quad (48)$$

Here, ψ is an integration constant which is $\pi/2$ for antiphase coupling. For small $\Delta\theta$, we find a first order transient response:

$$\Delta\theta \approx \Delta\theta_0 e^{-K_c t/A} + \frac{\pi}{2}. \quad (49)$$

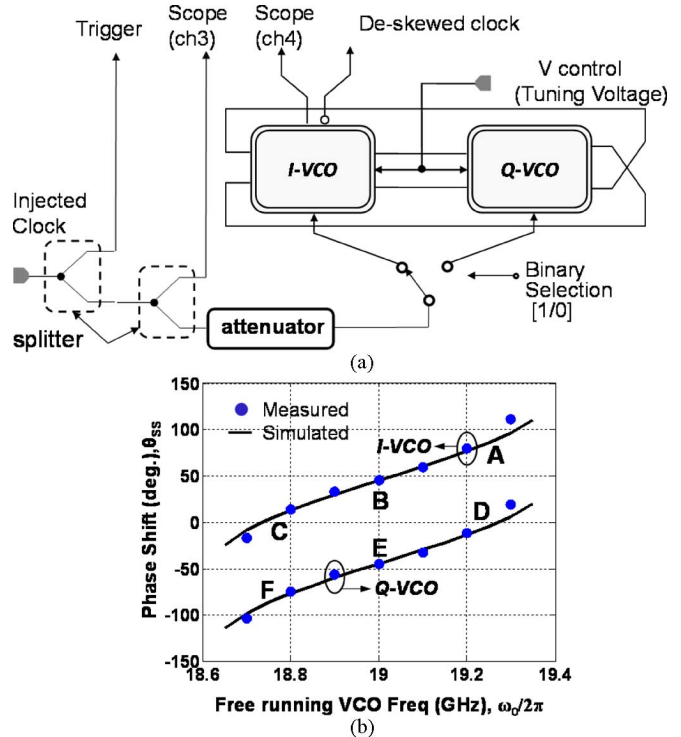


Fig. 20. Proposed phase deskew technique. (a) Experimental setup with Q VCO. (b) Corresponding deskew curve at $\omega_{inj} = 2\pi \times 19$ GHz and $K = 0.17$.

Here, $\Delta\theta_0$ is the initial phase difference at time $t = 0$. As $t \rightarrow \infty$, the phase difference $\Delta\theta$ exponentially approaches $\pi/2$. The significance of the of the above expression is that any jitter event in θ_I will be tracked with θ_Q (and vice versa) by

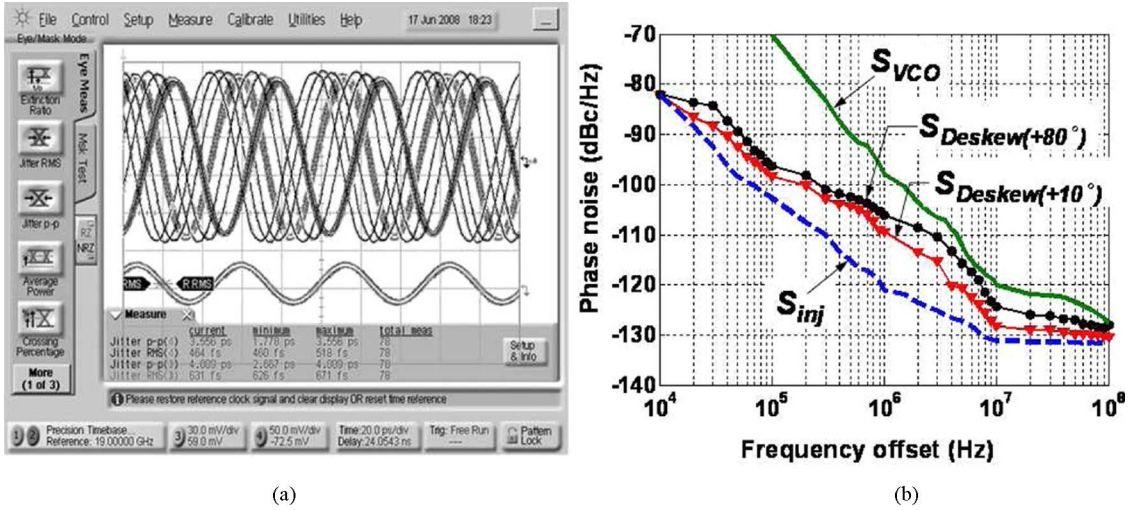


Fig. 21. Performance of proposed deskew technique. (a) Deskewed clock at different skew settings. (b) Corresponding measured phase noise $\omega_{inj} = 2\pi \times 19$ GHz.

a first order low pass response. The pole of this first order low pass response is

$$\omega_Q = \frac{K_c}{A}. \quad (50)$$

With that insight, now we can study the jitter transfer functions in the proposed deskew method shown in Fig. 18(b). To model the proposed deskew technique we consider two cases. First, phase noise at the output due to I-VCO injection (S_{I-out}) is observed. In this case, only in-phase injection (I_{Iinj}) is applied and I_{Qinj} is set to zero. Second, we consider the phase noise at the output due to Q-VCO injection (S_{Q-out}). In this case quadrature injection (I_{Qinj}) is applied and I_{Iinj} is set to zero. Similar to Section III(B), to derive a closed form expression, small injection strength and frequency offset are assumed, $K \ll 1$ and $\Delta\omega \ll \omega_{Lock}$. Following the method described in Section III(B), we can express the phase noise for I-VCO injection:

$$S_{I-out}(\omega_{jitter}) \approx \frac{\omega_P^2 S_{Iinj} + \omega_{jitter}^2 S_{VCO}}{\omega_P^2 + \omega_{jitter}^2}. \quad (51)$$

Note that ω_P is the pole due to external injection defined in (32). The case of injection at I-VCO is very similar to injection of a single-phase differential VCO. Thus the pole of the jitter transfer function is set by the external injection strength, K , as expressed in (32). However, jitter transfer function at the Q-VCO output will be a function of both ω_P and ω_Q . Since the Q-VCO output in turn injects back into the I-VCO, the coupling strength K_c can have a secondary influence on the ILO jitter transfer function, but this higher-order effect is safely ignored in the analysis as verified by simulations. However, in the case of Q-VCO injection, we need to take into account the second pole ω_Q and thus the phase noise can be expressed as

$$S_{Q-out}(\omega_{jitter}) \approx \frac{\omega_P^2 \omega_Q^2 S_{Q-inj} + \omega_{jitter}^2 (\omega_{jitter}^2 + \omega_P^2 + \omega_Q^2) S_{VCO}}{(\omega_{jitter}^2 + \omega_P^2)(\omega_{jitter}^2 + \omega_Q^2)}.$$

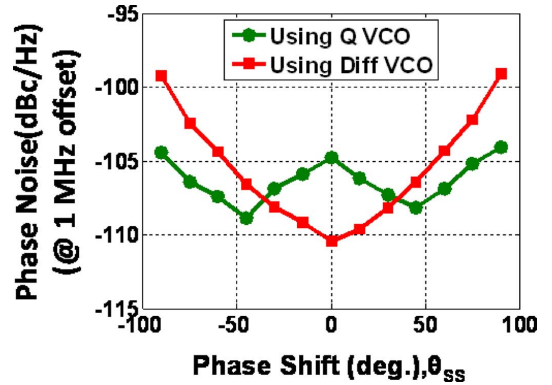


Fig. 22. Performance comparison: Phase noise @ 1 MHz offset for different skew angles $\omega_{inj} = 2\pi \times 19$ GHz.

(52)

The accuracy of the above two expressions are verified with the theoretical and simulated jitter transfer functions for I-VCO injection and Q-VCO injection shown in Fig. 19. When the coupling factor between the in-phase and quadrature VCOs is much stronger than that of the injection, $K_c \gg K$, $\omega_Q > \omega_P$ and the bandwidth of the jitter transfer function is mainly dominated by the ω_P . However, for larger injection strengths, the effect of ω_Q becomes prominent. Note that for small injection strength of $K = 0.085$, there is no noticeable change in JTJ where as for $K = 0.22$ Q-VCO injection results in about 50 MHz reduction in JTJ compared to I-VCO injection.

The proposed deskew technique utilizing an LC QVCO is shown in Fig. 20(a). The forwarded clock is injected to the in-phase VCO to achieve 0° to 90° phase shift only. For 0° to -90° , the injection is shifted to the quadrature VCO resulting in two deskew curves on Fig. 19(b). Thus we are using less than half of the lock range. Note that in the proposed QVCO based deskew scheme, we arbitrarily choose point C or D in the deskew curve as reference zero degree deskew. Since these two points have highest 200 MHz frequency offset from the free running VCO frequency, phase noise is also highest in

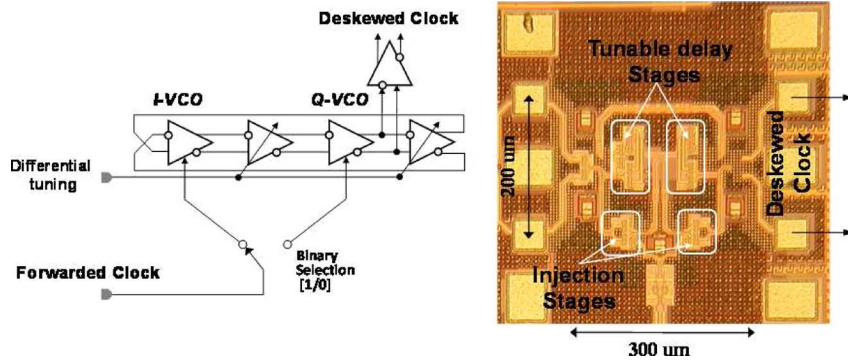


Fig. 23. Implementation of proposed deskew technique with a ring oscillator.

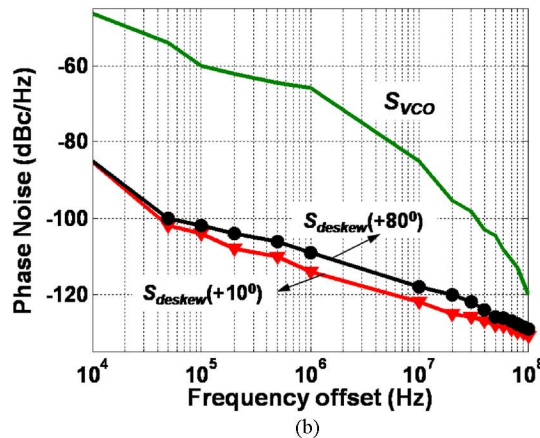
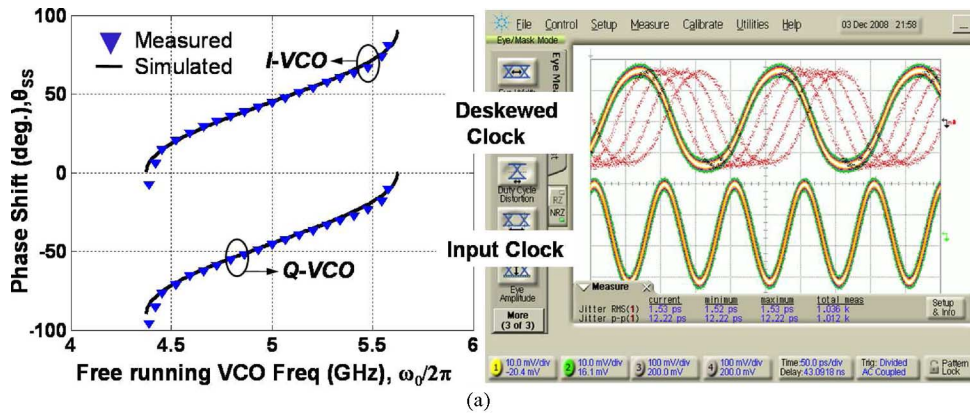


Fig. 24. (a) Generated skew curve as a function of free running frequency ($\omega_{inj} = 2\pi \times 10$ GHz and $K = 0.25$). (b) Measured Phase noise for $\theta_{ss} = 10^\circ$ and $\theta_{ss} = 80^\circ$.

these two points. On the other hand, point *B* and *E* is used as $+45^\circ$ and -45° deskew respectively. Since the frequency offset is zero, lowest phase noise is achieved. Variation of the jitter tracking bandwidth with frequency offset (hence, deskew) is nonlinear (Fig. 15). For example, if $K=0.17$, a frequency offset of 150 MHz cause only 50 MHz reduction in JTB. It turns out that amplitude variation is also minimal in that range. Thus, the proposed technique allows us to accomplish -90° to $+90^\circ$ phase selection with linear phase steps and negligible amplitude variation, as shown in Fig. 21(a). Note that point *D* and *A* on the deskew curve Fig. 20(b) represents 0° and 90° phase shift. In the proposed technique, these two deskew angles are obtained by setting same frequency offset

(200 MHz) and by switching the injection node from I-VCO to Q-VCO. As discussed earlier, switching the injection node from I-VCO to Q-VCO has little effect on JTB if $\omega_p \ll \omega_Q$. As a result only small variation of the phase noise of the deskewed clock is observed in Fig. 21(b). For comparison with a simple differential injection-locked VCO, the phase noise at 1 MHz offset is plotted versus deskew angle in Fig. 22 which verifies the advantage of the proposed technique. In the worst case condition ($+90^\circ$ or -90°) 8 dB of phase noise improvement is obtained. Note that in the plot of Fig. 21 the reference phase angle of 0° is shifted by 45° in the Q-VCO case so that both plots cover the same $\pm 90^\circ$ range.

In a practical system, phase selection can be performed as in a conventional phase-locked or delay-locked loop. For example, in [26] the ILO output is compared to a reference clock by a phase detector which in turn drives a loop filter that tunes the ILO. In a data recovery system, a data-driven phase detector would be required. Eventually the loop converges to a point either on the curve $A \rightarrow C$ or $D \rightarrow F$. Note that these two curves have overlap which may cause ambiguity in the control logic. For example, 0 phase deskew can be achieved either by choosing the point C or D. This problem can easily be solved by adding hysteresis in the control logic.

B. Deskew With Ring Oscillator

If the link needs to support wide range of data rates, ring oscillators are often preferred over LC-VCOs due to their wide tuning range. The proposed deskew technique is easily realizable for those applications. From Table III, increasing the number of stages provides more nodes for injection thus the opportunity to restrict $\Delta\omega$ over a narrower range providing more linear phase adjustment. On the other hand, fewer stages provides lower power consumption and higher jitter tracking bandwidth. As a proof of concept, a four stage ring oscillator implemented in 90 nm CMOS is used in this study. The oscillator provides a tuning range from 2 GHz-7 GHz. The injection signal is at $2f_{osc}$ (Fig. 23). Similar to the LC oscillator, phase deskew curves for both in-phase and quadrature injection are shown in Fig. 24. The effects of quadrature injection on jitter filtering and amplitude variations are very similar to the LC oscillator case.

V. CONCLUSION

In summary, a low power clock source that incorporates a buffer into a cross-coupled oscillator has been demonstrated. By isolating the load from the tank, the oscillator can directly drive 50-Ohm impedances or large capacitive loads with no additional buffering. A QVCO using this topology in 0.13 μm digital CMOS oscillates at 20 GHz, consumes 20 mW and provides 12% tuning range with a measured phase noise is -101 dBc/Hz @ 1 MHz frequency offset. Injection-locked QVCOs are particularly useful as deskew elements in high-speed parallel links. By selectively injecting different phases of a quadrature-LC or ring VCO, variations in the ILO's jitter tracking bandwidth are muted and phase noise can be reduced. For a fixed data rate, LC oscillators can provide lower phase noise whereas ring oscillators are preferred for variable data rates. Due to the additional VCO stages in quadrature, this technique will consume more power compared to [6] and [7]. The technique is demonstrated using a LC QVCO at 20 GHz while burning only 20 mW of power and providing an 8 dB improvement in phase noise. A ring oscillator deskews a 2 to 7 GHz clock while consuming 14 mW in 90 nm CMOS. These figures still compare favorably with using a complete DLL for deskewing. In addition, ILOs are more immune to supply noise and duty cycle distortion.

APPENDIX

In the case of a ring oscillator, the VCO transfer function is low pass. Assume the ring oscillator is implemented with n

identical stages. Each stage had a dc gain of H_o and single pole ω_P . Thus the equivalent transfer function can be written as

$$H(j\omega) = \frac{H_o^n}{(1 + j\frac{\omega}{\omega_P})^n}. \quad (53)$$

Considering the positive feedback introduces 180° phase shift, the remaining phase shift required to ensure oscillation at ω_o is

$$\Phi|_{\omega=\omega_o} = \angle(H(j\omega_o)) = -n \tan^{-1} \left(\frac{\omega_o}{\omega_P} \right) = -\pi \quad (54)$$

$$\tan \left(\frac{\pi}{n} \right) = \frac{\omega_o}{\omega_P}. \quad (55)$$

Substituting (55) into (53)

$$H(j\omega) = \frac{H_o^n}{\left(1 + j\frac{\omega}{\omega_o} \tan \left(\frac{\pi}{n} \right)\right)^n} \quad (56)$$

$$\Phi = -n \tan^{-1} \left(\frac{\omega}{\omega_o} \tan \left(\frac{\pi}{n} \right) \right). \quad (57)$$

Substituting this into (21) gives

$$A = - \frac{\tan \left[n \tan^{-1} \left(\frac{\omega}{\omega_o} \tan \left(\frac{\pi}{n} \right) \right) \right]}{\omega_o - \omega}. \quad (58)$$

Adopting the approximation in (26) gives

$$\begin{aligned} A &= - \frac{d \tan \Phi}{d\omega} \Big|_{\omega=\omega_o} = \frac{n \tan \left(\frac{\pi}{n} \right)}{\omega_o \sec^2 \left(\frac{\pi}{n} \right)} \sec^2 \Phi \Big|_{\omega=\omega_o} \\ &= \frac{n \tan \left(\frac{\pi}{n} \right)}{\omega_o \sec^2 \left(\frac{\pi}{n} \right)} = \frac{n}{2\omega_o} \sin \left(\frac{2\pi}{n} \right). \end{aligned} \quad (59)$$

ACKNOWLEDGMENT

The authors would like to acknowledge F. O'Mahony, M. Mansuri, and B. Casper of the Intel Circuits Research Lab at Hillsboro, Oregon, for their contribution to the clock deskew technique presented in this work.

REFERENCES

- [1] H. Takauchi *et al.*, "A CMOS multichannel 10-Gb/s transceiver," *IEEE J. Solid-State Circuits*, vol. 38, no. 12, pp. 2094–2100, Dec. 2003.
- [2] B. Casper *et al.*, "A 20 Gb/s forwarded clock transceiver in 90-nm CMOS," in *IEEE ISSCC Dig. Tech. Papers*, 2006, pp. 90–91.
- [3] F. O'mahony *et al.*, "A low-jitter PLL and repeaterless network for a 20 Gb/s link," in *IEEE Symp. VLSI Circuits Dig.*, 2006.
- [4] R. Kreienkamp *et al.*, "A 10-Gb/s CMOS clock and data recovery circuit with an analog phase interpolator," *IEEE J. Solid-State Circuits*, vol. 40, no. 3, pp. 736–743, Mar. 2005.
- [5] C. Kromer *et al.*, "A 25-Gb/s cdr in 90-nm CMOS for high-density interconnects," *IEEE J. Solid-State Circuits*, vol. 41, no. 12, pp. 2921–2929, Dec. 2006.
- [6] L. Zhang, B. Ciftcioglu, M. Huang, and H. Wu, "Injection-locked clocking: A new GHz clock distribution scheme," presented at the IEEE Custom Integrated Circuits Conf., San Jose, CA, Sep. 2006.
- [7] F. O'Mahony *et al.*, "A 27 Gb/s forwarded clock I/O receiver using an injection-locked LC-DCO in 45 nm CMOS," in *IEEE ISSCC Dig.*, 2008.

- [8] M. Tiebout, "Low power low-phase-noise differentially tuned quadrature VCO design in standard cmos," *IEEE J. Solid-State Circuits*, vol. 36, no. 5, pp. 1018–1024, May 2001.
- [9] D. Ham and A. Hajimiri, "Concepts and methods in optimization of integrated LC VCOs," *IEEE J. Solid-State Circuits*, vol. 36, no. 6, pp. 896–909, Jun. 2001.
- [10] K. Kwok and J. Long, "A 23-to-29 GHz transconductor-tuned VCO MMIC in 0.13 μm CMOS," *IEEE J. Solid-State Circuits*, vol. 42, no. 12, pp. 2878–3997, Dec. 2007.
- [11] N. Nguyen and R. G. Meyer, "Start up and frequency stability in high-frequency oscillators," *IEEE J. Solid-State Circuits*, vol. 27, no. 5, pp. 810–820, May 1992.
- [12] R. Aparicio and A. Hajimiri, "A noise-shifting differential Colpitts VCO," *IEEE J. Solid-State Circuits*, vol. 37, no. 12, pp. 1728–1736, Dec. 2002.
- [13] K. W. Tang *et al.*, "Frequency scaling and topology comparison of mm-wave CMOS VCOs," in *Proc. IEEE CSICS*, Nov. 2006, pp. 55–58.
- [14] A. Lacatia, S. Levantino, and C. Samori, *Integrated Frequency Synthesizers for Wireless Systems*, 1st ed. Cambridge, UK: Cambridge Univ. Press, 2007, pp. 86–95.
- [15] *International Technology Roadmap of Semiconductors*, ITRS, 2003 [Online]. Available: www.itrs.org
- [16] S. Li, I. Kipnis, and M. Ismail, "A 10-GHz CMOS quadrature LC-VCO for multicore optical applications," *IEEE J. Solid-State Circuits*, vol. 38, no. 10, pp. 1626–1634, Oct. 2003.
- [17] F. Ellinger and H. Jäckel, "38-43 ghz quadrature vco on 90 nm vlsi cmos with feedback frequency tuning," in *IEEE MTT-S Int. Microwave Symp. Dig.*, 2005, p. 3.
- [18] H. R. Rategh and T. H. Lee, "Superharmonic injection-locked frequency dividers," *IEEE J. Solid-State Circuits*, vol. 34, no. 6, pp. 813–821, Jun. 1999.
- [19] H. Ng *et al.*, "A second-order semidigital clock recovery circuit based on injection locking," *IEEE J. Solid-State Circuits*, vol. 38, no. 12, pp. 2101–2110, Dec. 2003.
- [20] R. Adler, "A study of locking phenomena in oscillators," *Proc. IRE*, vol. 33, pp. 351–357, Jun. 1946.
- [21] L. J. Paciore, "Injection locking of oscillators," *Proc. IEEE*, vol. 53, no. 11, pp. 1723–1728, Nov. 1965.
- [22] M. Mansuri *et al.*, "Strong injection locking of low-q lc oscillators," presented at the IEEE Custom Integrated Circuits Conf., San Jose, CA, Sep. 2008.
- [23] B. Razavi, "A study of injection locking and pulling in oscillators," *IEEE J. Solid-State Circuits*, vol. 39, no. 9, pp. 1415–1424, Sep. 2004.
- [24] X. Zhang, X. Zhou, B. Aliener, and A. S. Daryoush, "A study of subharmonic injection locking for local oscillators," *IEEE Microwave Guided Wave Lett.*, vol. 2, pp. 97–99, Mar. 1992.
- [25] A. Mirzaei, M. Heidari, R. Bagheri, S. Chehrizi, and A. Abidi, "The quadrature LC oscillator: A complete portrait based on injection locking," *IEEE J. Solid-State Circuits*, vol. 42, no. 9, pp. 1916–1932, Sep. 2007.
- [26] J. Lee, H. Wang, W. Chen, and Y. Lee, "Subharmonically injection-locked pll's for ultra-low-noise clock generation," in *IEEE ISSCC Dig.*, 2009.



Masum Hossain received the B.Sc. degree in electrical engineering from Bangladesh University of Engineering and Technology, Bangladesh, and the M.Sc. degree from Queen's University, Canada, in 2002 and 2005, respectively. During his M.Sc., he worked on K-band wireless receiver in CMOS. Since 2005, he has been working towards the Ph.D. degree in electrical engineering at University of Toronto.

From September 2007 to January 2008, he was with Intel Circuit Research Lab (CRL) as a graduate intern. Currently, he is working for Gennum Corp. in the Analog and Mixed Signal division. His research interests include mixed signal circuits for high-speed chip-to-chip communications, low power VCO, phase interpolator and clock recovery techniques. He won the Best Student Paper Award at the 2008 Custom Integrated Circuits (CICC) conference.



Anthony Chan Carusone (S'96–M'02–SM'08) received the B.A.Sc. and Ph.D. degrees from the University of Toronto in 1997 and 2002, respectively, during which time he received the Governor-General's Silver Medal.

Since 2001, he has been with the Department of Electrical and Computer Engineering at the University of Toronto where he is currently an Associate Professor. In 2008 he was a visiting researcher at the University of Pavia, Italy, and later at the Circuits Research Lab of Intel Corp., Hillsboro, Oregon.

Prof. Chan Carusone was a co-author of the best paper at the 2005 Compound Semiconductor Integrated Circuits Symposium and the best student papers at both the 2007 and 2008 Custom Integrated Circuits Conferences. He is an appointed member of the Administrative Committee of the IEEE Solid-State Circuits Society, a member and past chair of the Analog Signal Processing Technical Committee for the IEEE Circuits and Systems Society, and a member and past chair of the Wireline Communications subcommittee of the Custom Integrated Circuits Conference. He serves as a guest editor for both the *IEEE JOURNAL OF SOLID-STATE CIRCUITS* and the *IEEE TRANSACTIONS ON CIRCUITS AND SYSTEMS I: REGULAR PAPERS*. He is currently Editor-in-Chief of the *IEEE TRANSACTIONS ON CIRCUITS AND SYSTEMS II: EXPRESS BRIEFS*.